nature medicine

A novel human primary immunodeficiency syndrome caused by deficiency of the endosomal adaptor protein p14

Georg Bohn[1], Anna Allroth[1], Gudrun Brandes[2] Jens Thiel[3], Erik Glocker[3], Alejandro A Schäffer[4], Chozhavendan Rathinam[1], Nicole Taub[5], David Teis[5], Cornelia Zeidler[1], Ricardo A Dewey[1], Robert Geffers[6], Jan Buer[6], Lukas A Huber[5], Karl Welte[1], Bodo Grimbacher[3,7,8] & Christoph Klein[1,8]

Lysosome-related organelles have versatile functions, including protein and lipid degradation, signal transduction and protein secretion. The molecular elucidation of rare congenital diseases affecting endosomal-lysosomal biogenesis has given insights into physiological functions of the innate and adaptive immune system. Here, we describe a previously unknown human primary immunodeficiency disorder and provide evidence that the endosomal adaptor protein p14, previously characterized as confining mitogen-activated protein kinase (MAPK) signaling to late endosomes, is crucial for the function of neutrophils, B cells, cytotoxic T cells and melanocytes. Combining genetic linkage studies and transcriptional profiling analysis, we identified a homozygous point mutation in the 3′ untranslated region (UTR) of *p14* (also known as *MAPBPIP*), resulting in decreased protein expression. In p14-deficient cells, the distribution of late endosomes was severely perturbed, suggesting a previously unknown role for p14 in endosomal biogenesis. These findings have implications for understanding endosomal membrane dynamics, compartmentalization of cell signal cascades, and their role in immunity.

The study of human primary immunodeficiency disorders has advanced our understanding of basic host defense[1]. In particular, the molecular analysis of a group of human diseases giving rise to defects in both pigmentation and immune function has provided insights into the biology of secretory lysosomes, specialized organelles containing proteins that can be released upon external stimulation[2]. Chédiak-Higashi syndrome[3,4], Griscelli syndrome type 2 (refs. 5,6) and Hermansky-Pudlak syndrome type 2 (refs. 7,8) are caused by defects in proteins controlling lysosomal secretion in immune cells and melanocytes. Individual components governing the fate of lysosomal organelles are emerging, yet a comprehensive understanding of the versatile functions of endosomes and lysosomes remains elusive. Although distinct routes of membrane trafficking have been identified in the biogenesis of lysosomal organelles[9–13], their physiological significance remains controversial. Furthermore, an important role for lysosomes in the spatiotemporal control of cell-surface receptor–mediated signal transduction is increasingly being recognized[14,15].

Here we describe a previously unknown primary immunodeficiency syndrome comprising congenital neutropenia, partial albinism, short stature and B-cell and cytotoxic T-cell deficiency. We provide evidence that the disease is caused by deficiency of the late endosomal-lysosomal MEK binding partner 1 (MP1)-interacting protein (also known as p14, HSPC003 and MAPBPIP), an adaptor molecule orchestrating the subcellular anatomy of MAP kinase signaling[16–18]. Furthermore, we define a previously unknown role for p14 in the biogenesis of endosomes.

RESULTS

Clinical and pathological phenotype

Four out of 15 offspring of a white Mennonite index family showed a characteristic clinical phenotype associating short stature, hypopigmented skin, coarse facial features and recurrent bronchopulmonary infections by *Streptococcus pneumoniae* (**Fig. 1a–c**). All participants had constantly low peripheral neutrophil counts (absolute neutrophil count (ANC) $< 500/\mu l$), although neutrophil maturation in the bone marrow was intact (**Fig. 1d,e**). Low-dose granulocyte-colony stimulating factor (G-CSF) therapy reconstituted normal peripheral neutrophil levels (**Fig. 1e**). T cells were present in normal numbers and responded adequately to mitogens and recall antigens (**Supplementary Table 1** online). The total number of $CD19^+$ B cells was increased in all subjects

[1]Department of Pediatric Hematology/Oncology and [2]Department of Cell Biology, Hannover Medical School, Carl Neuberg Strasse 1, D-30625 Hannover, Germany. [3]Division of Rheumatology and Clinical Immunology, University Hospital Freiburg, Hugstetterstrasse 55, D-79106 Freiburg, Germany. [4]National Center for Biotechnology Information, National Institutes of Health, Department of Health and Human Services, 8600 Rockville Pike, Bethesda, Maryland 20894, USA. [5]Biocenter, Division of Cell Biology, Medical University of Innsbruck, Fritz-Pregl Strasse 3, A-6020 Innsbruck, Austria. [6]Helmholtz Centre for Infection Research (HCI), Array Facility and Mucosal Immunity, Inhoffenstrasse 7, D-38124 Braunschweig, Germany. [7]Present address: Department of Immunology and Molecular Pathology, Royal Free Hospital, University College London, Pond Street, London NW3 2QG, UK. [8]These authors contributed equally to this work. Correspondence should be addressed to C.K. (klein.christoph@mh-hannover.de).

Received 10 July; accepted 23 November; published online 31 December 2006; doi:10.1038/nm1528

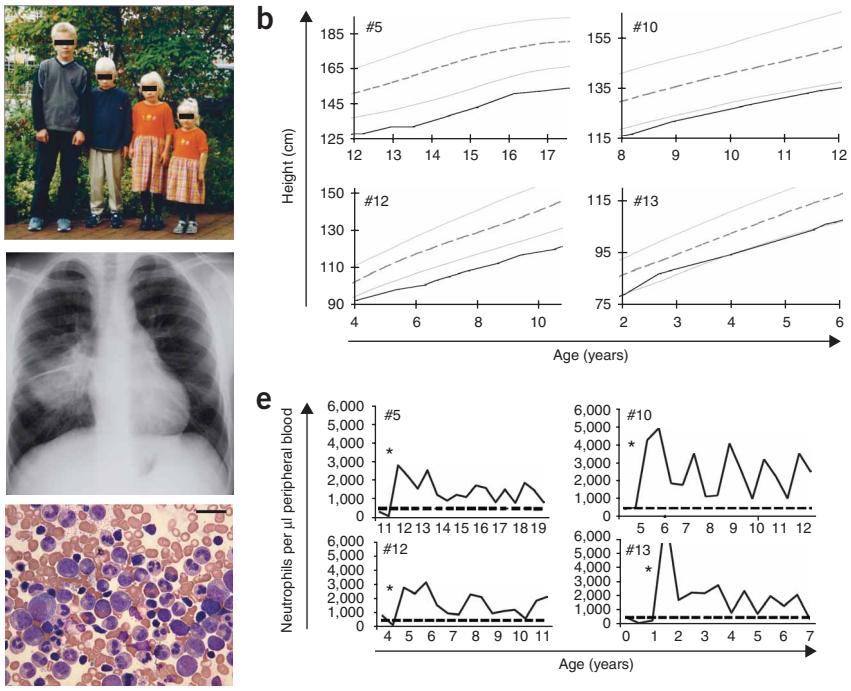

Figure 1 Clinical presentation. (**a**) Phenotype of sujbects, with hypopigmentation of hair and skin. (**b**) Growth profiles of subjects (black curves). 97th, 50th and 3rd percentiles are shown as gray lines. (**c**) Chest radiograph of subject #5 suffering from *Streptococcus pneumoniae* infection. (**d**) Representative bone marrow smear prior to initiation of G-CSF therapy. There is a predominance of myeloid cells and the presence of neutrophils. Scale bar, 5 μm. (**e**) Peripheral blood neutrophil counts over time. All subjects suffered from severe congenital neutropenia (dotted line, 500 neutrophils/μl) which was responsive to administration of G-CSF. Asterisk indicates start of G-CSF treatment.

(**Fig. 2a**). Although the percentage of naive $IgD^+IgM^+CD27^-$ B cells was increased, the percentages of $IgD^+IgM^+CD27^+$ memory B cells and $IgD^-IgM^-CD27^+$ class-switched memory B cells were reduced in all subjects (**Fig. 2a** and **Supplementary Table 1**). Furthermore, all subjects showed consistently reduced serum IgM levels, and two subjects developed low IgG levels in their adolescence (**Supplementary Table 1**).

The clinical phenotype associating immunodeficiency and hypopigmentation is reminiscent of genetic diseases caused by defects in secretory lysosomes[2], such as Chédiak-Higashi syndrome[3,4], Hermansky-Pudlak syndrome (HPS) type 2 (refs. 7,8) or Griscelli syndrome type 2 (refs. 5,6). But the combination of clinical features could not easily be reconciled with any of these disorders. For example, none of these three syndromes has been reported to include short stature as part of the phenotype. In an attempt to better delineate this disorder, we undertook further studies to elucidate the function of cells containing specialized

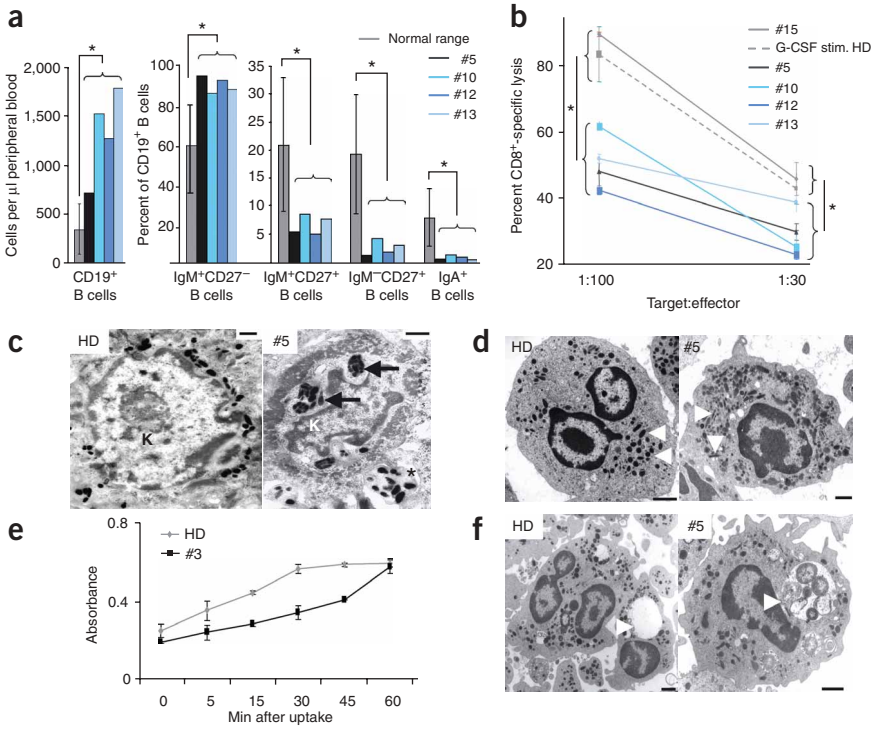

Figure 2 Phenotype of immune cells and melanocytes. (**a**) Immunophenotype of peripheral blood B cells. Left, absolute numbers of $CD19^+$ B cells. Right, percentage of naive $IgD^+IgM^+CD27^-$ B cells (IgM^+CD27^-), $IgD^+IgM^+CD27^+$ memory B cells (IgM^+CD27^+), $IgD^-IgM^-CD27^+$ class-switched memory B cells (IgM^-CD27^+) and IgA^+ B cells. $^*P < 0.05$. (**b**) Cytotoxic T-cell (CTL) function assessed by ^{51}Cr release assay. CTLs from a healthy sibling (#15) and a healthy donor (HD) treated with G-CSF served as controls. $^*P < 0.05$. (**c**) TEM of skin kerotinocytes. Left, normal distribution of mature melanosomes in a skin keratinocyte (K) of a healthy donor (HD). Single mature melanosomes are grouped separately around the nucleus. Right, abnormal melanosome distribution in skin keratinocyte (K) of subject #5. There is agglomeration of immature melanosomes in large phagosomes (arrows). Asterisks indicate melanocyte process with normal melanosomes at various maturation stages. Scale bar, 0.5 μm. (**d**) TEM of neutrophil granulocytes. Left, healthy donor (HD). Right, subject #5. Note the abnormal elongated shape of azurophilic granules in the subject's granulocyte (arrows). Similar changes were seen in all four subjects (see **Supplementary Fig. 1**). Scale bar, 1 μm. (**e**) Intracellular lysis of *E. coli*. Purified neutrophils were exposed to *E. coli* and lysis of the bacterial membrane was measured by fluorimetric β-Gal assay (absorbance at 420 nm). (**f**) TEM of neutrophils upon phagocytosis of *P. aeruginosa*. Phagosomes of the subject's neutrophils are filled with undigested debris (arrow, right panel), whereas bacteria in healthy control neutrophils (HD) were almost completely digested (arrow, left panel). Scale bar, 1 μm.

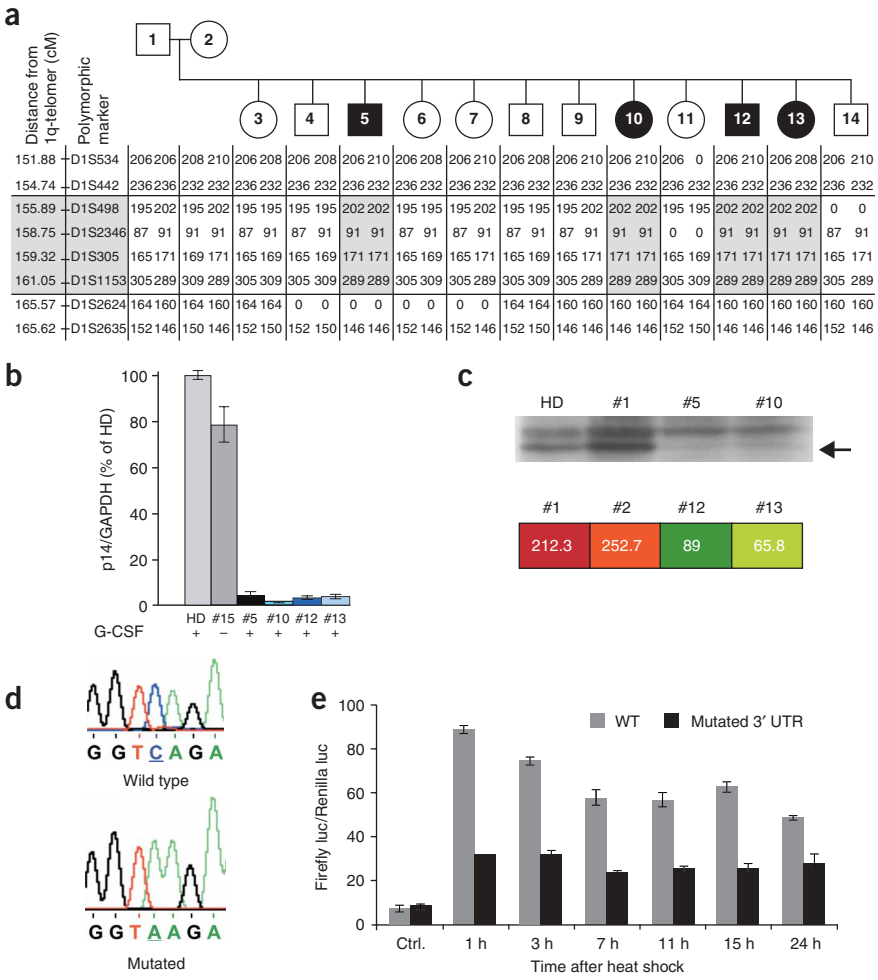

Figure 3 Haplotypes, mutational analysis and determination of RNA instability. (**a**) Allele distribution in subjects (black) and healthy family members (white). The homozygous linkage interval on chromosome 1q21 including the *p14* gene is shown in gray. For details, see **Supplementary Methods**. (**b**) mRNA quantification of *p14* in neutrophils by RT-PCR analysis in healthy control individuals (G-CSF–treated HD and healthy sibling #15). (**c**) Upper panel, western blot analysis of p14 in EBV-transformed B-cell lines from healthy control (HD), unaffected family member #1 and two subjects (#5, 10). Arrow indicates p14-specific band corresponding to 25 kDa protein. Lower panel, expression intensities of transcripts in EBV-transformed B-cell lines derived from parents (#1, 2) compared to subjects (#12, 13). For a complete list of differentially regulated genes, see **Supplementary Table 3** online. (**d**) Sequencing of *p14* 3′ UTR showing a single base change (C → A). (**e**) Luciferase assay showing decreased enzymatic activity in the presence of the mutated 3′ UTR. Wild-type (WT) and mutated 3′ UTR sequences were cloned into heat shock–inducible luciferase reporter constructs as described in **Supplementary Methods**. Upon transient transfection of the reporter constructs, transcription was induced by heat shock for 1 h and luciferase activity was determined at indicated time points ($P < 0.001$ at all time points).

lysosome-related organelles such as cytotoxic T cells (CTLs), melanocytes and neutrophil granulocytes.

CTLs kill target cells by a mechanism requiring a coordinated release of prestored cytotoxic granules upon cellular stimulation and activation of death receptors[19,20]. To functionally characterize CTLs, we determined their cytotoxic activity against the Fas-insensitive target cell line L1210. Compared to cells of healthy siblings, $CD8^+$ CTLs from all participants had decreased cytotoxic activity (**Fig. 2b**), suggesting that assembly and/or release of granules containing cytotoxic proteins might be disturbed. We did not, however, detect any defect in docking, fusion and secretion of secretory lysosomes (**Supplementary Fig. 1** online), indicating that the vectorial movement and focused secretion of cytotoxic protein granules remained intact. Accordingly, the release of granzyme B was unaffected (**Supplementary Fig. 1**). Furthermore, perforin and its unprocessed precursor forms were detectable in CTLs as shown by immunofluorescence and western blotting (**Supplementary Fig. 1**).

Melanocytes are a nonhematopoietic cell type characterized by the presence of secretory granules destined to produce melanin. Using transmission electron microscopy (TEM), we analyzed the pigment pattern in participants' epidermal skin. In contrast to samples from healthy individuals, participants' immature melanosomes were accumulated and immediately degraded upon transfer into basal keratinocytes, suggesting that the coordinated maturation of melanosomes was disrupted (**Fig. 2c**). On a cellular level, these findings provide an explanation for the hypopigmented phenotype.

Neutrophil granulocytes contain lysosome-like organelles called azurophilic granules, which fuse with phagosomes and thus facilitate degradation of phagocytosed particles. We used TEM studies to characterize density and shape of granules in neutrophils. In contrast to normal control neutrophils, azurophilic granules in the subjects' neutrophils formed electrodense slender tubules. The overall density of granules appeared normal (**Fig. 2d** and **Supplementary Fig. 2** online). In view of the structural abnormalities in the lysosomal compartment of neutrophils, we next performed a series of functional studies. Phagocytosis of bacteria was unaffected in the subjects' neutrophils, as assessed by uptake of fluorescence-labeled *Escherichia coli* and subsequent FACS analysis (data not shown). To monitor lysis of ingested bacteria in phagosomes, we made use of a particular strain of *E. coli* (ML-35, $laci^-z^+y^-$)[8,21]. Upon engulfment of *E. coli* ML-35 by neutrophils, the bacterial wall is perforated in the phagosomes and releases β-galactosidase (β-Gal), whose enzymatic activity can be measured by a photometric assay. *In vitro*–generated neutrophils from a healthy control donor showed effective lysis of ML-35 cells, whereas neutrophils from subject #5 showed markedly delayed lytic activity (**Fig. 2e**). We confirmed these data using TEM studies of mature neutrophils exposed to pathogenic *Pseudomonas aeruginosa* particles. The fusion of lysosomes and phagosomes appeared intact, but the bacteria were eliminated less efficiently in the phagosomes from subjects compared to neutrophils from healthy control individuals (**Fig. 2f**). Finally, we undertook electron microscopy studies to analyze platelet dense granules, a lysosome-related organelle typically defective in HPS. We did not see any abnormality,

however (data not shown). Together, the clinical and pathological phenotype of this novel immunodeficiency syndrome seemed to be associated with an abnormal maturation and function of specialized lysosomes in cytotoxic T cells, melanocytes and neutrophil granulocytes.

Linkage analysis and mutational analysis

To identify the genetic basis of this syndrome, we carried out a genome-wide genetic linkage study. As the family belongs to a religious isolate, we expected that the disease would be associated with a homozygous mutation in a single gene. We performed the genome scan on the parents and 12 siblings, 4 affected and 8 of the 11 unaffected siblings (**Fig. 3a**). After we had genotyped 188 markers spread among all 22 autosomes, we examined the data for promising regions. No marker among these segregated perfectly, but we found nine markers with a logarithm of odds (LOD) score > 1 in model 1 (assuming no consanguinity) and five markers with a LOD score > 1 in model 2 (assuming consanguinity). Three of these high-scoring markers, all on chromosome 1, were common to the two sets. Marker D1S1679 had scores of +1.49 in model 1 and +1.22 in model 2 partly because the adjacent marker D1S1589 also had positive scores (**Supplementary Table 2** online). It should be noted that marker D1S1589 achieves its peak scores at $\theta = 0$ partly because it is not fully informative in this pedigree. Multipoint analysis suggested that the disease gene was likely to lie above D1S1679, not at D1S1589 or between the two markers. Multipoint linkage analysis gave a peak score of +2.80 for model 1 and a peak score of +4.39 for model 2; the curves are absolutely flat within 0.05 of the peak score for any placement of the putative disease gene between D1S498 and D1S1553 (**Supplementary Table 2**). If one adds in the subsequently obtained information that the three unaffected siblings not used in the genome scan are also not homozygous in the linkage region, then the LOD score for model 1 rises to 3.17. As model 1 assumes no consanguinity, our claim of linkage to chromosome 1 does not rest on this unproven assumption.

We identified four perfectly segregating markers on chromosome 1: D1S498, D1S2346, D1S305 and D1S1153 (**Fig. 3a** and **Supplementary Table 2**). Within the maximal possible linkage region, there were 192 genes or predicted genes, including *p14*.

As our initial efforts to find mutations in a series of potential candidate genes (**Supplementary Table 2**) were not successful, we next performed a genome-wide transcriptional profiling screen in EBV-transformed B-cell lines using high-density Affymetrix microarray analysis. Combining the results of the linkage analysis with the transcriptional profiling approach, only one gene located within the crucial region on chromosome 1q21 was underexpressed by a factor of >2 in the subjects, namely *p14* (**Fig. 3c** and **Supplementary Table 3** online). This finding was confirmed by RT-PCR analysis using cDNA from multiple tissues such as primary granulocytes (**Fig. 3b,c**), EBV-transformed B-cell lines and fibroblasts (data not shown). As expected, western blot analysis showed substantially reduced p14 protein expression levels in B cells from subjects compared to control B cells (**Fig. 3c**). No mutation in the coding regions of *p14* could be detected. All affected family members (#5, 10, 12 and 13; **Fig. 3a**), however, had a homozygous mutation in the 3′ untranslated region (UTR) in exon 4. At position +23 from the lower exon boundary, the nucleotide adenosine was replaced by cytidine (**Fig. 3d**). Sequencing results from the parents and phenotypically healthy family members showed a heterozygous mutation at this locus in the parents and family members 7, 9 and 14, whereas in the wild-type sequence was present in the other family members. Screening of 100 control alleles ruled out that the detected change is a polymorphism. Moreover, we ruled out that this genomic change is characteristic for the Mennonite population by sequencing 34 alleles from healthy Mennonites, which were all identical to the wild-type sequence.

Implications of the 3′ UTR point mutation on RNA levels

We reasoned that the point mutation in the 3′ UTR might either create an alternative splice site or affect proper polyadenylation of the mRNA. We saw no alternative transcripts in northern blot analysis, however, and the length of the poly-A tail was not altered in the presence of the 3′ UTR point mutation (data not shown). To directly assess whether the point mutation in the subjects' 3′ UTR leads to decreased RNA stability, we generated luciferase expression constructs driven by heat

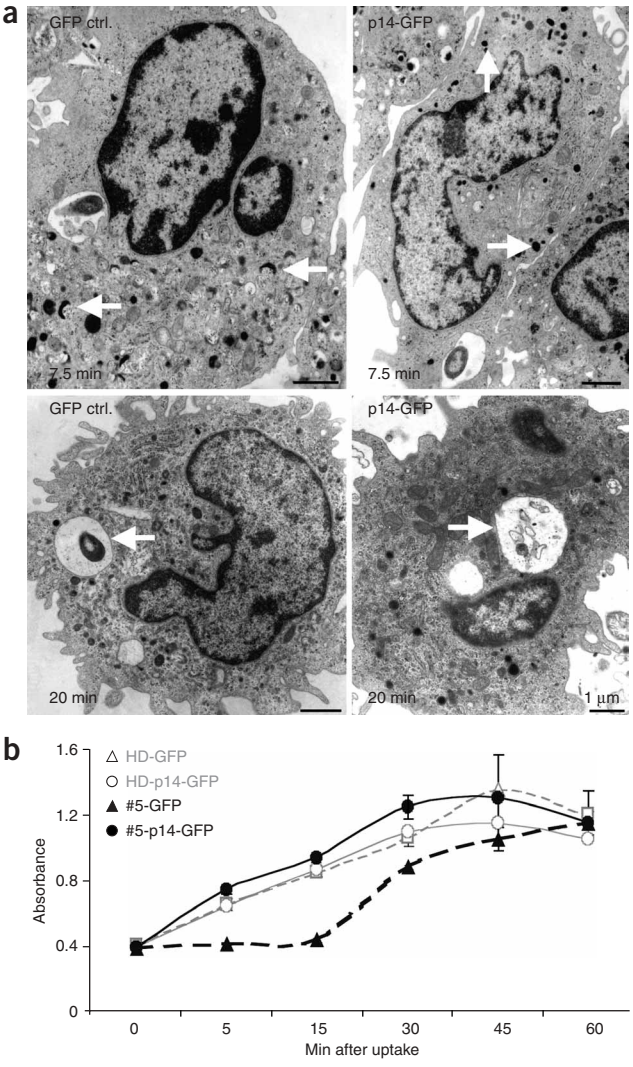

Figure 4 Reconstitution of lysosome-related organelles in neutrophils upon retroviral *p14* gene transfer. (**a**) TEM of *in vitro*–generated neutrophil granulocytes after ingestion of *P. aeruginosa* (for details, see **Supplementary Methods**). Azurophilic granules are indicated by arrows in upper panels (7.5 min), phagosomes are indicated by arrows in lower panels (20 min). Left, control transduced cells. Right, p14-transduced cells. (**b**) Intracellular lysis of *E. coli* in *in vitro*–generated retrovirus-transduced neutrophils from subject #5 and a healthy donor (HD). For statistical analysis, see **Supplementary Figure 2**.

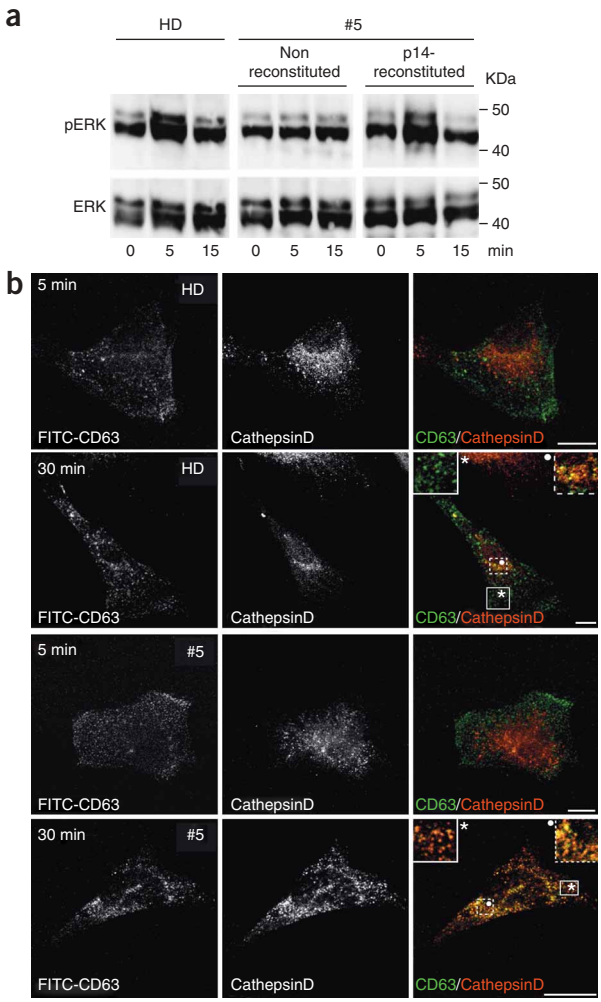

Figure 5 Defective signal transduction and late endosomal distribution in p14-deficient fibroblasts. (**a**) Western blot analysis showing G-CSF–induced ERK phosphorylation in G-CSFR–expressing fibroblasts. Serum-starved cells from a healthy donor (HD) and a subject (#5) were stimulated with recombinant human G-CSF and harvested at the indicated time points for detection of pERK (upper) and ERK (lower). p14 reconstitution status of cells as indicated. (**b**) Immunofluorescence study showing subcellular distribution of late endosomes in control (HD) and p14-deficient (#5) fibroblasts (original magnification, ×63). Cells were continuously chased for the indicated time with FITC-conjugated CD63 (LAMP3)-specific monoclonal antibodies (green fluorescence) and costained with cathepsin D–specific antibodies (red fluorescence) to visualize late endosomes. Left panels show green fluorescence signals, middle panels show red fluorescence signals and right panels show colocalization of red and green signals. Insets show enlarged peripheral and perinuclear area, respectively. Scale bar, 10 μm.

shock–inducible promoters. Firefly luciferase was stabilized either by participant or wild-type 3′ UTR, respectively. Upon cotransfection of the firefly and Renilla luciferase into Chinese hamster ovary (CHO) cells and subsequent promoter induction, we lysed the cells and determined the luciferase activity by luminometry. Luciferase activity was consistently reduced in cells transfected with constructs containing the mutated *p14* 3′ UTR, suggesting that the point mutation destabilized the RNA (**Fig. 3e**). These experiments suggest that decreased p14 protein expression is due to decreased RNA stability, but further studies are necessary to document the molecular pathophysiology in greater detail. p14 deficiency thus represents an additional example of genetic diseases associated with 3′ UTR mutations[22].

Functional reconstitution upon *p14* gene transfer

To provide definitive proof that *p14* is the causative gene accounting for the clinical phenotype of these subjects, we attempted to functionally reconstitute the abnormal azurophilic granules in neutrophils by retroviral gene transfer. We purified $CD34^+$ hematopoietic progenitor cells from participants and healthy donors and transduced them with retroviral vectors encoding p14 and green fluorescent protein (GFP) in a bicistronic construct, or GFP alone, respectively. Upon *in vitro* differentiation into mature neutrophils, we exposed the cells to *P. aeruginosa* and analyzed them by TEM at various time points. As expected, control-transduced neutrophils showed an aberrant configuration of azurophilic granules and a deficiency in clearing the bacteria in phagosomes. In contrast, p14-reconstituted neutrophils showed a normal granule pattern and an increased lytic capacity of phagosomes (**Fig. 4a**). More importantly, we also showed reconstitution of defective *E. coli* lysis upon *p14* gene transfer in a fluorometric assay (**Fig. 4b**). Thus, p14 is directly responsible for the neutrophil dysfunction in these subjects.

Functional effects of decreased p14 levels

p14 represents an adaptor molecule previously thought to be involved in the localization of the MP1-MAPK scaffold complex to endosomes[16,17]. Scaffold and adaptor molecules diversify the signaling cascades by assembling specific signaling complexes to distinct subcellular locations. For example, the extracellular signal-regulated (ERK) protein cascade is specified by two known scaffold proteins. The kinase suppressor of RAS (KSR1) enhances ERK activation at the plasma membrane, and MEK1 partner (MP1) orchestrates ERK signaling at the endosome as a result of its interaction with p14. Subcellular compartmentalization through adaptor molecules such as p14 may not only control the dynamics of receptor downregulation and degradation but also distinct cellular responses to cell-surface receptor signaling[14,15]. Intrigued by the phenotype of congenital neutropenia in our subjects, we hypothesized that the granulocyte colony–stimulating factor receptor (G-CSFR) signal, most relevant for the generation[23] and release[24] of mature neutrophil granulocytes, might be affected in p14-deficient cells. To assess the G-CSFR signal cascade in p14-deficient cells, we made of use of fibroblasts transduced with retroviral vectors encoding a G-CSFR–GFP fusion construct[25] (for further characterization of cells see **Supplementary Fig. 3** online). We stimulated the cells with recombinant G-CSF, and assessed the downstream MAPK signal cascade by western blot analysis of ERK phosphorylation. ERK phosphorylation was reduced in the absence of p14 and was reconstituted upon retroviral *p14* gene transfer (**Fig. 5a**), suggesting that the intracellular G-CSFR–dependent signal transduction is partly controlled by p14.

In view of the characteristic cellular deficiency in cells with specialized lysosomal compartments, we hypothesized that p14 might have a previously unrecognized role in the biogenesis of lysosomes.

Two distinct pathways of lysosomal biogenesis have been recognized. In the 'direct' pathway, membranes bud from the trans-Golgi network and fuse with endosomes. Alternatively, membrane constituents can be shuttled into endosomes through the plasma membrane following the 'indirect' pathway[9,10]. The limiting membrane of lysosomes contains lysosome-associated membrane proteins (LAMPs), targeted to lysosomes by virtue of adaptor-protein complexes.

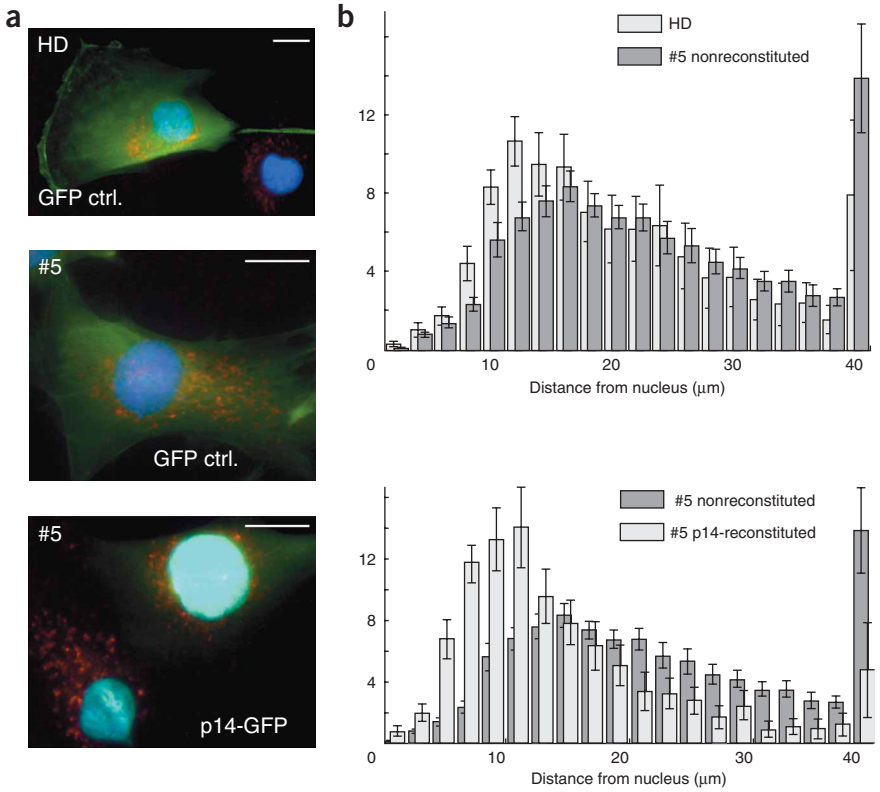

Figure 6 Aberrant subcellular distribution of late endosomes in p14-deficient fibroblasts and reconstitution upon retroviral gene transfer. (**a**) Immunofluorescence analysis showing subcellular distribution of late endosomes. Control fibroblasts (HD) were GFP control transduced (GFP crtl., upper panel), subject's fibroblasts (#5) were transduced either with GFP (GFP ctrl., middle) or with p14-GFP–encoding retroviral constructs (lower panel). Late endosomes are stained with cathepsin D–specific antibodies (red signal). Scale bar, 10 μm. (**b**) Semiquantitative analysis measuring the frequency distribution of late endosomes (*y* axis) in defined distances to the nucleus (*x* axis, $n = 15$ cells). Details are described in **Supplementary Methods**. A chi-square independence test was performed on the original data (sum of all endosomes per bin) for HD versus #5 nonreconstituted (upper), for #5 nonreconstituted versus #5 reconstituted (lower), and for HD versus #5 reconstituted (data not shown). Endosome distance distributions were found to be different at the $P < 0.001$ level for all three cases, normal (GFP ctrl.) versus participant (GFP ctrl.) cells, participant (GFP ctrl.) versus rescue (patient, GFP-p14) and normal (GFP ctrl.) versus rescue (patient, GFP-p14).

To visualize trafficking of LAMPs to late endosomes through the indirect pathway, we chased p14-deficient and control fibroblasts using FITC-conjugated LAMP3 (CD63)-specific antibodies and analyzed them using fluorescence microscopy. We took images 5 and 30 min after exposure to CD63-specific antibodies, respectively, and identified late endosomes by costaining them with cathepsin D–specific antibodies. At 5 min, both control fibroblasts and p14-deficient fibroblasts showed uptake of FITC-conjugated CD63-specific antibodies in the early endosomal compartment, located in the periphery of the cells (**Fig. 5b**). At 30 min, we observed colocalization of CD63-specific and cathepsin D–specific antibodies both in control and in p14-deficient fibroblasts, suggesting that the late endosomal compartment was reached independently of the abundance of p14. However, although control fibroblasts showed a predominantly perinuclear accumulation of late endosomes (**Fig. 5b**), p14-deficient cells showed a wide distribution of late endosomes throughout the cytoplasm. A semiquantitative analysis of the nuclear-endosomal distance (**Supplementary Fig. 4** online) suggests that the subcellular architecture of the late endosomal compartment is perturbed in the absence of p14. To unequivocally prove that this effect is specifically dependent on p14, we also performed retroviral gene transfer studies and analyzed the distribution of cathepsin D–positive late endosomes in p14- and control-transduced fibroblasts. p14-deficient control-transduced fibroblasts showed a scattered distribution pattern of cathepsin D–positive late endosomes, which could be reverted to the typical perinuclear wildtype pattern upon retroviral *p14* gene transfer (**Fig. 6**; $P < 0.001$, see **Supplementary Methods** online). These findings indicate that p14 controls the configuration of the late endosomal compartment.

DISCUSSION

We identified a novel complex primary immunodeficiency syndrome caused by a homozygous point mutation in the 3′ UTR of *p14*, leading to decreased RNA stability, decreased protein levels and aberrant lysosomal function. p14 deficiency resembles known lysosomal diseases associating partial albinism and immunodeficiency, such as Chédiak-Higashi syndrome (LYST deficiency)[3,4], Griscelli syndrome type 2 (RAB27A deficiency)[5,6] or Hermansky-Pudlak syndrome type 2 (HPS2, AP3B1 deficiency)[7,8]. The clinical phenotype can easily be distinguished, however, as short stature is not typically seen in any of these disorders. A pathognomonic feature of Chédiak-Higashi syndrome is the presence of characteristic inclusion bodies in neutrophils, which were not seen in p14-deficient participants. People with Griscelli syndrome type 2 typically present with hemophagocytic lymphohistiocytosis resulting from characteristic defects in cytotoxic granule exocytosis[6], which could not be seen in p14-deficient CTLs. In contrast to p14 deficiency, HPS2 is not associated with defects in B and T cells. Thus, clinical and immunological features allow a nosological discrimination of p14 deficiency.

Our study is the first to describe the phenotype of a hypomorphic 'p14 knockdown' and thus provides further insights in the biological function of p14. Mice with a targeted deletion of p14 are not viable[26], suggesting that p14 is of crucial importance in early embryonal development. Previously, p14 has been shown to be crucial for epidermal growth factor receptor (EGFR)-mediated signaling and the spatiotemporal control of ERK1/2 phosphorylation[17]. Our analysis of reduced G-CSFR–mediated ERK1/2 phosphorylation in p14-deficient cells extends this finding and suggests that cytokine receptor signaling in general may depend on p14-dependent proper subcellular localization of endosomes. The abnormal distribution pattern of late endosomes in p14-deficient cells is very similar to findings in mouse p14-deficient embryonic fibroblasts[26] and thus documents a role for p14 in the biogenesis of late endosomes.

Despite our conclusive evidence of a p14-specific cellular phenotype, several issues require further studies. For example, we cannot

easily explain why people with a p14 deficiency are neutropenic. G-CSF–mediated signals, including ERK1/2 phosphorylation, are crucial to release mature neutrophils[24,27], but at this time there is no definitive proof that deficient G-CSFR signaling accounts for the neutropenia. In contrast to neutrophils from individuals with severe congenital neutropenia[28–31], we detected no increased susceptibility to apoptosis (data not shown). Furthermore, the underlying mechanisms of defective B and CTL function remain obscure. In contrast to defective exocytosis in LYST[32,33] and Rab27A deficiciency[6,34,35], we could not show any defect in granule release in p14-deficient CTLs. A possible hypothesis to explain this phenomenon may be that defective lysosomal maturation of secretory lysosomes is responsible for defective CTL function in p14-deficient individuals. We expect that further mechanistic insights into the defective function of hematopoietic cells will be gained by analysis of conditional p14-deficient mice[26].

In conclusion, we here describe a novel immunodeficiency disease associated with aberrant lysosomal function. Our studies will have important implications for the understanding of disease-associated 3′ UTR–mediated RNA processing, lysosomal membrane dynamics and endosomal signal transduction.

METHODS

Participants. We took blood samples and skin biopsies with informed consent. The study was approved by the Institutional Review Boards at Hannover Medical School and the University of Freiburg.

Genotyping and linkage analysis. We genotyped an initial set of microsatellite markers and an additional set of markers for fine mapping (**Supplementary Table 2**) on DNA extracted from whole blood (Gentra Systems) with the published PCR conditions (UCSC genome browser, http://genome.ucsc.edu), run on an ABI377 sequencer and analyzed with Genotyper software (Applied Biosystems). We checked genotype data for incompatibilities using the program PedCheck[36]. We computed LOD scores with the software package FASTLINK[37–39] using the pedigree as a nuclear family with no ancestors or inbreeding (Model 1) and alternatively, assuming that the parents are second cousins (Model 2). More information is available in **Supplementary Methods**.

Cells, antibodies and flow cytometry. A complete list and details of FACS analysis are available in **Supplementary Methods**.

Functional neutrophil studies. We purified primary granulocytes by gradient centrifugation over Ficoll Paque (Amersham Biosciences) and consecutive hypotonic erythrocyte lysis, yielding a purity of >95%, as assessed by Giemsa-stained cytospin preparations. In some experiments, we differentiated neutrophils from purified $CD34^+$ cells following previously published protocols[40]. We determined lysis of *E. coli* lysis using a lactose permease–deficient mutant strain of *E. coli* according to previously published protocols[21]. For electron microscopic studies, we incubated 10^6 neutrophils with 3×10^7 *P. aeruginosa* (gift from B. Tümmler, Hannover Medical School, Hannover, Germany), pelleted them and fixed them with 2.5% glutaraldehyde (Polysciences) in 0.1 M sodium cacodylate, pH 7.3 (Merck Schuchardt). Further details are in **Supplementary Methods**.

Cell lines, sequencing, western blotting, RNA and microarray studies. Cell lines, sequencing, western blotting, RNA and microarray studies are described in **Supplementary Methods**.

Immunofluorescence. We grew fibroblasts on glass cover slips (Menzel Glaeser), fixed them in 4% paraformaldehyde in 1× cytoskeletal buffer (CB) (2× CB: 20 mM) PIPES (pH 6.8), 300 mM NaCl, 10 mM EGTA, 10 mM glucose, 10 mM $MgCl_2$) permeabilized them with 0.2% Triton X-100, and incubated them with mouse antibody to human cathepsin D (clone M1G8, Schering; 400 ng/ml in gelatine blocking buffer). We washed cells and incubated them with secondary Alexa-568 goat anti-mouse antibody (Molecular Probes/Invitrogen), followed by 100 ng/ml DAPI solution (Molecular Probes/Invitrogen) and mounted them in Mowiol (Carl Roth). Assessment of endosome-nucleus distances is described in **Supplementary Methods**. For the CD63 chase experiment, we labeled fibroblasts with FITC-conjugated CD63-specific antibody (clone H5C6, BD Pharmingen) in a 1:10 dilution in medium containing 0.1% BSA, and then continuously chased at 37 °C and 5% CO_2. At indicated time points, we washed the cells, fixed them with 4% paraformaldehyde and stained them for cathepsin D as decribed above. We performed fluorescence microscopy with an LSM 510 Meta Axiovert 200 (Zeiss) and analyzed data using the corresponding software.

Luciferase assay. We modified the pGL3 basic vector (Promega GmbH) to drive luciferase transcription from a human HSP70 promoter. The SV40 poly-A signal was replaced by the *p14* 3′ UTR sequence from participants (containing the point mutation) or healthy controls, respectively. An HSP70-driven renilla luciferase expression vector served as transfection control. We cotransfected plasmids at a ratio of 1:50 into CHO cells using Lipofectamine reagent (Invitrogen). We heated cells at 42 °C for 1 h. We measured firefly and renilla luciferase activity in protein lysates using a commercially available kit system (Promega).

Retroviral gene transfer experiments. We cloned human *p14* cDNA into the bicistronic retroviral vector MMP[41] containing either GFP or mCD24 as a marker gene. We generated gibbon ape leukemia virus (GALV) envelope–pseudotyped retroviruses by tripartite transient transfection of MMP-based transfer vectors together with the envelope plasmid K83.pHCMV-GALVenv (gift from C. Baum, Hannover Medical School, Hannover, Germany) and the packaging plasmid pMD.old.gag/pol into the cell line 293T. In some experiments, we generated VSV-G–pseudotyped retroviruses using transient transfection into the packaging cell line 293GPG as previously described[42]. We transduced purified $CD34^+$ cells as described in **Supplementary Methods**. A retroviral transfer vector encoding G-CSFR was obtained from I. Touw, Rotterdam, The Netherlands[25].

Statistical analysis. We compared participant and reference values using Student *t*-test, and computed nonparametric 95% confidence intervals for the median for these parameters. We performed computations using SAS (Statistical Analysis System Version 9.1, SAS Institute Inc). For details, see **Supplementary Methods**.

Accession codes. GenBank accession code: *p14*, NM_01417.

Note: Supplementary information is available on the Nature Medicine website.

ACKNOWLEDGMENTS

We thank M. Schlesier (University of Freiburg) for the B-cell phenotyping, I. Sandrock, G. Köhne, F. Noyan, K. Boztug and M. Ballmaier for laboratory support, C. Roifman (Hospital for Sick Children) and R. Gatti (University of California at Los Angeles) for providing control samples on Mennonite families, and E. Ungewickell, C. Baum, J. Bohne, C. Kardinal and H. Holtmann for critical discussions. We thank B. Tümmler (Hannover Medical School), C. Baum (Hannover Medical School) and I. Touw (Erasmus University Medical Center) for reagents, M. Zimmermann for help in statistical evaluations and M. Offterdinger for help in determining subcellular distribution of endosomes. This research was supported by Deutsche Forschungsgemeinschaft grants KFO110 and GR1617/3, BMBF, the Elternverein Krebskranke Kinder Hannover, the Austrian Proteomics Platform (APP, GEN-AU), the Special Research Program "Cell Proliferation and Cell Death in Tumors" (SFB021, Austrian Science Fund) and in part by the intramural research program of the US National Institutes of Health, National Library of Medicine (NLM).

AUTHOR CONTRIBUTIONS

A.A., G. Brandes and J.T. contributed equally to this work. G. Bohn sequenced candidate genes and performed most molecular and cellular functional studies. A.A. characterized the 3′ UTR mutation by assessing RNA metabolism and functional reporter assays. G. Brandes performed electron microscopy and immunofluorescence studies. J.T. performed fine-mapping, screened candidate genes and helped to edit the manuscript. E.G. performed the genome-wide scan. A.A.S. carried out the genetic linkage analysis computations, chose the markers for genetic linkage fine mapping and wrote parts of the manuscript. C.R. performed *E. coli* lysis assays. N.T. and D.T. did immunofluorescence studies on endosomes. C.Z. cared for patients, and collected and curated data in SCN patient registry. R.A.D. assisted Bohn, A.A. and C.R. R.G. and J.B. performed

microarray experiments. L.A.H. gave advice on endosome biology, and educated and supervised N.T. and D.T. K.W. provided laboratory resources, resources for SCN registry and significant help to initiate and carry out the study. B.G. initiated the project together with C.K., educated and supervised J.T. and E.G., assisted A.A.S. in linkage analysis, provided grant and laboratory resources and edited the manuscript. C.K. designed and directed the study, obtained clinical samples, taught and supervised Bohn, A.A., C.R. and R.A.D., provided laboratory and financial resources and wrote the manuscript.

COMPETING INTERESTS STATEMENT

The authors declare that they have no competing financial interests.

Published online at http://www.nature.com/naturemedicine
Reprints and permissions information is available online at http://npg.nature.com/reprintsandpermissions/

1. Fischer, A. Human primary immunodeficiency diseases: a perspective. *Nat. Immunol.* **5**, 23–30 (2004).
2. Stinchcombe, J., Bossi, G. & Griffiths, G.M. Linking albinism and immunity: the secrets of secretory lysosomes. *Science* **305**, 55–59 (2004).
3. Barbosa, M.D.F.S. *et al.* Identification of the homologous *beige* and Chediak-Higashi syndrome genes. *Nature* **382**, 262–265 (1996).
4. Nagle, D.L. *et al.* Identification and mutation analysis of the complete gene for Chediak-Higashi syndrome. *Nat. Genet.* **14**, 307–311 (1996).
5. Klein, C. *et al.* Partial albinism with immunodeficiency (Griscelli syndrome). *J. Pediatr.* **125**, 886–895 (1994).
6. Ménasché, G. *et al.* Mutations in *RAB27A* cause Griscelli syndrome associated with haemophagocytic syndrome. *Nat. Genet.* **25**, 173–176 (2000).
7. Dell'Angelica, E.C., Shotelersuk, V., Aguilar, R.C., Gahl, W.A. & Bonifacino, J.S. Altered trafficking of lysosomal proteins in Hermansky-Pudlak syndrome due to mutations in the β3A subunit of the AP-3 adaptor. *Mol. Cell* **3**, 11–21 (1999).
8. Jung, J. *et al.* Identification of a homozygous deletion in the *AP3B1* gene causing Hermansky-Pudlak syndrome, type 2. *Blood* **108**, 362–369 (2006).
9. Kornfeld, S. & Mellman, I. The biogenesis of lysosomes. *Annu. Rev. Cell Biol.* **5**, 483–525 (1989).
10. Janvier, K. & Bonifacino, J.S. Role of the endocytic machinery in the sorting of lysosome-associated membrane proteins. *Mol. Biol. Cell* **16**, 4231–4242 (2005).
11. Bonifacino, J.S. & Glick, B.S. The mechanisms of vesicle budding and fusion. *Cell* **116**, 153–166 (2004).
12. Ghosh, P., Dahms, N.M. & Kornfeld, S. Mannose 6-phosphate receptors: new twists in the tale. *Nat. Rev. Mol. Cell Biol.* **4**, 202–212 (2003).
13. Gruenberg, J. & Stenmark, H. The biogenesis of multivesicular endosomes. *Nat. Rev. Mol. Cell Biol.* **5**, 317–323 (2004).
14. Mor, A. & Philips, M.R. Compartmentalized Ras/MAPK signalling. *Annu. Rev. Immunol.* **24**, 771–800 (2006).
15. Kolch, W. Coordinating ERK/MAPK signalling through scaffolds and inhibitors. *Nat. Rev. Mol. Cell Biol.* **6**, 827–837 (2005).
16. Wunderlich, W. *et al.* A novel 14-kilodalton protein interacts with the mitogen-activated protein kinase scaffold mp1 on a late endosomal/lysosomal compartment. *J. Cell Biol.* **152**, 765–776 (2001).
17. Teis, D., Wunderlich, W. & Huber, L.A. Localization of the MP1-MAPK scaffold complex to endosomes is mediated by p14 and required for signal transduction. *Dev. Cell* **3**, 803–814 (2002).
18. Kurzbauer, R. *et al.* Crystal structure of the p14/MP1 scaffolding complex: how a twin couple attaches mitogen-activated protein kinase signaling to late endosomes. *Proc. Natl. Acad. Sci. USA* **101**, 10984–10989 (2004).
19. Russell, J.H. & Ley, T.J. Lymphocyte-mediated cytotoxicity. *Annu. Rev. Immunol.* **20**, 323–370 (2002).
20. Trambas, C.M. & Griffiths, G.M. Delivering the kiss of death. *Nat. Immunol.* **4**, 399–403 (2003).
21. Hamers, M.N., Bot, A.A., Weening, R.S., Sips, H.J. & Roos, D. Kinetics and mechanism of the bactericidal action of human neutrophils against *Escherichia coli*. *Blood* **64**, 635–641 (1984).
22. Chen, J.-M., Férec, C. & Cooper, D.N. A systematic analysis of disease-associated variants in the 3′ regulatory regions of human protein-coding genes I: general principles and overview. *Hum. Genet.* **120**, 1–21 (2006).
23. Souza, L.M. *et al.* Recombinant human granulocyte colony-stimulating factor: effects on normal and leukemic myeloid cells. *Science* **232**, 61–65 (1986).
24. Semerad, C.L., Liu, F., Gregory, A.D., Stumpf, K. & Link, D.C. G-CSF is an essential regulator of neutrophil trafficking from the bone marrow to the blood. *Immunity* **17**, 413–423 (2002).
25. Aarts, L.H.J., Roovers, O., Ward, A.C. & Touw, I.P. Receptor activation and 2 distinct COOH-terminal motifs control G-CSF receptor distribution and internalization kinetics. *Blood* **103**, 571–579 (2004).
26. Teis, D. *et al.* p14-MP1-MEK1 signaling regulates endosomal traffic and cellular proliferation during tissue homeostasis. *J. Cell Biol.* (in the press).
27. Price, T.H., Chatta, G.S. & Dale, D.C. Effect of recombinant granulocyte colony-stimulating factor on neutrophil kinetics in normal young and elderly humans. *Blood* **88**, 335–340 (1996).
28. Carlsson, G. *et al.* Kostmann syndrome: severe congenital neutropenia associated with defective expression of Bcl-2, constitutive mitochondrial release of cytochrome *c*, and excessive apoptosis of myeloid progenitor cells. *Blood* **103**, 3355–3361 (2004).
29. Klein, C. *et al.* Deficiency of HAX1 causes severe congenital neutropenia (Kostmann disease). *Nat. Genet.* (in the press).
30. Köllner, I. *et al.* Mutations in neutrophil elastase causing congenital neutropenia lead to cytoplasmic protein accumulation and induction of the unfolded protein response. *Blood* **108**, 493–500 (2006).
31. Zhuang, D., Qiu, Y., Kogan, S.C. & Dong, F. Increased CCAAT enhancer-binding protein epsilon (C/EBPepsilon) expression and premature apoptosis in myeloid cells expressing Gfi-1 N382S mutant associated with severe congenital neutropenia. *J. Biol. Chem.* **281**, 10745–10751 (2006).
32. Huynh, C., Roth, D., Ward, D.M., Kaplan, J. & Andrews, N.W. Defective lysosomal exocytosis and plasma membrane repair in Chediak-Higashi/beige cells. *Proc. Natl. Acad. Sci. USA* **101**, 16795–16800 (2004).
33. Baetz, K., Isaatz, S. & Griffiths, G.M. Loss of cytotoxic T lymphocyte function in Chediak Higashi syndrome arises from a secretory defect that prevents lytic granule exocytosis. *J. Immunol.* **154**, 6122–6131 (1995).
34. Haddad, E.K., Wu, X., Hammer, J.A., III. & Henkart, P.A. Defective granule exocytosis in Rab27a-deficient lymphocytes from *ashen* mice. *J. Cell Biol.* **152**, 835–842 (2001).
35. Stinchcombe, J. *et al.* Rab27a is required for regulated secretion in cytotoxic T lymphocytes. *J. Cell Biol.* **152**, 825–834 (2001).
36. O'Connell, J.R. & Weeks, D.E. PedCheck: A program for identification of genotype incompatibilities in linkage analysis. *Am. J. Hum. Genet.* **63**, 259–266 (1998).
37. Lathrop, G.M. & Lalouel, J.-M. Easy calculations of LOD scores and genetic risks on small computers. *Am. J. Hum. Genet.* **36**, 460–465 (1984).
38. Cottingham, R.W., Idury, R.M., Jr. & Schäffer, A.A. Faster sequential genetic linkage computations. *Am. J. Hum. Genet.* **53**, 252–263 (1993).
39. Schäffer, A.A., Gupta, S.K., Shriram, K. & Cottingham, R.W., Jr. Avoiding recomputation in linkage analysis. *Hum. Hered.* **44**, 225–237 (1994).
40. Hino, M. *et al. Ex vivo* expansion of mature human neutrophils with normal functions from purified peripheral blood $CD34^+$ haematopoietic progenitor cells. *Br. J. Haematol.* **109**, 314–321 (2000).
41. Klein, C., Bueeler, H. & Mulligan, R.C. Comparative analysis of genetically modified dendritic cells and cytokine transduced tumor cells as therapeutic cancer vaccines. *J. Exp. Med.* **191**, 1699–1708 (2000).
42. Ory, D.S., Neugeboren, B.A. & Mulligan, R.C. A stable human-derived packaging cell line for production of high titer retrovirus/vesicular stomatitis virus G pseudotypes. *Proc. Natl. Acad. Sci. USA* **93**, 11400–11406 (1996).